



One-Step Phosphine-Oxide Post-Modification of Multi-Resonance Emitters for Efficient, Narrowband, Quenching-Resistant OLEDs

Lixiao Guo, Weibo Cui, Yexuan Pu, Linjie Li, Yuhan Sun, Pingping Zheng, Chenglong Li,* and Yue Wang

Abstract: Multiple-resonance thermally activated delayed fluorescence (MR-TADF) materials featuring high efficiency and narrowband emission are crucial for wide color-gamut organic light-emitting diodes (OLEDs), but they often suffer from complex synthesis and limited structural diversity. In this study, we report a one-step, metal-free phosphine-oxide (P=O) post-modification strategy to construct the first B/N/P=O fused MR-TADF emitters, PO-BCzBN and PO-tFBN. This strategy introduces a covalent P=O lock, enhancing the rigidity of the π -conjugation plane to maintain narrowband emission while simultaneously suppressing aggregation-caused quenching (ACQ) through the steric hindrance introduced by the trigonal pyramidal geometry of sp^3 -hybridized P atom. PO-BCzBN and PO-tFBN show photoluminescence emission peaks at 466 and 493 nm with narrow full widths at half maximum (FWHMs) of 21 and 23 nm in solution, near-unity photoluminescence quantum yields of 98% and 99%, rapid reverse intersystem crossing rates of 2.0×10^4 and 2.1×10^4 s⁻¹, and suppressed concentration quenching in films. Sensitizer-free OLEDs based on PO-BCzBN and PO-tFBN achieve maximum external quantum efficiencies of 21.6%–34.2% (electroluminescence emission peaks, λ_{ELS} = 472–476 nm, FWHMs = 24–28 nm) and 28.3%–35.8% (λ_{ELS} = 496–500 nm, FWHMs = 26–27 nm) across a broad doping range (1–20 wt%), respectively, demonstrating superior resistance to spectral broadening and ACQ.

Introduction

The metal-free thermally activated delayed fluorescence (TADF) materials enable 100% exciton utilization through

the up-conversion of triplet excitons, making them highly promising candidates for the development of high-efficiency organic light-emitting diodes (OLEDs). However, the large structural differences between the ground-state (S_0) and the lowest singlet state (S_1) in twisted donor-acceptor (D-A) type TADF materials result in broad full width at half-maximum (FWHM, > 70 nm).^[1–3] To address this issue, Hatakeyama et al. in 2016 proposed a novel molecular design paradigm, namely multiple-resonance TADF (MR-TADF).^[4] Electron-deficient boron (B) and electron-rich nitrogen (N) atoms are doped in para-positions of polyaromatic hydrocarbons (PAHs), leading to an alternating distribution of the highest occupied molecular orbital (HOMO) and lowest unoccupied molecular orbital (LUMO) and rigid π -conjugation, which suppresses the exchange interaction between frontier molecular orbitals (FMOs) and excited-state structural relaxation. Therefore, TADF property and narrowband emission are achieved for MR-TADF materials.^[5–13] Currently, the construction of B/N-based MR-TADF materials predominantly follows a de novo synthesis strategy, in which borylated precursors are designed through retrosynthetic analysis and subsequently transformed into target compounds via two main borylation approaches: one-pot and one-shot borylation.^[14–21] The one-pot borylation method involves an organolithium-mediated borylation-annulation reaction, which enables the precise synthesis of target molecules by pre-installing halogen substituents in the borylated precursors.^[22–28] In contrast, the one-shot borylation method enables the direct construction of borylated products via intra- and intermolecular bora-Friedel–Crafts (BFC) reactions. With precise tuning of electronic and steric effects, this approach has emerged as a complementary strategy that eliminates the need for pre-installed halogen substituents or organolithium reagents.^[29–33] Both approaches have been extensively developed and have jointly accelerated the advancement of MR-TADF materials, leading to the realization of numerous high-efficiency, narrowband-emitting OLED devices. Nevertheless, the de novo synthesis of MR-TADF molecules via borylation strategies still encounters several challenges, such as the delicate design of precursors and control of reaction sites, and often involves time-consuming procedures when optimizing molecular properties.^[34,35]

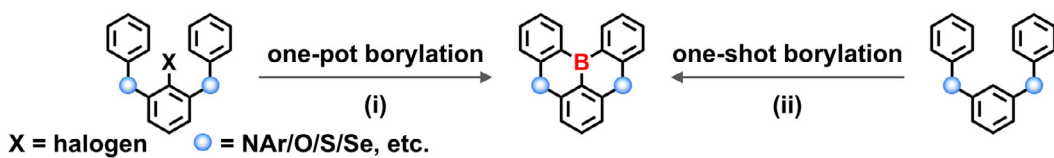
In this context, post-modification strategies provide a powerful and complementary approach, enabling precise tuning of molecular properties and broadening structural diversification by introducing functional groups at peripheral or selectively reactive sites on preassembled molecular

[*] L. Guo, W. Cui, Y. Pu, L. Li, Y. Sun, P. Zheng, Prof. C. Li, Prof. Y. Wang
 State Key Laboratory of Supramolecular Structure and Materials,
 College of Chemistry, Jilin University, Changchun 130012, P. R. China
 E-mail: chenglongli@jlu.edu.cn

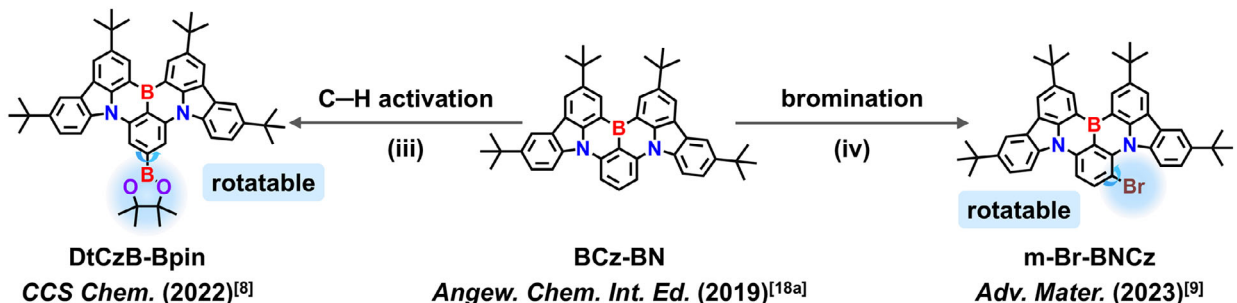
Prof. Y. Wang
 Jihua Laboratory, 28 Huandao South Road, Foshan, Guangdong
 Province 528200, P. R. China

Additional supporting information can be found online in the Supporting Information section

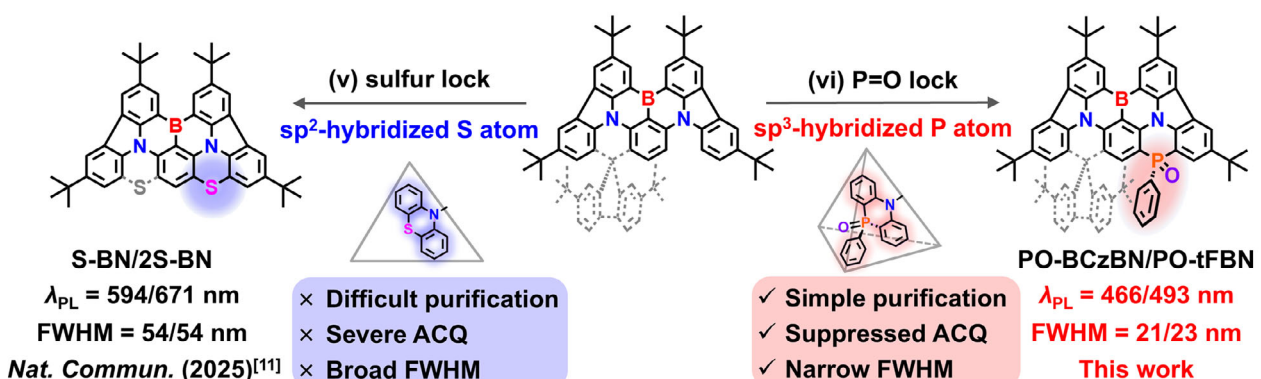
a) De novo synthesis strategy



b) Intermediate-mediated post-modification strategy



c) One-step post-modification strategy



Scheme 1. The molecular synthesis strategies for the MR-TADF emitters of a) De novo synthesis: i) $n\text{-BuLi}$ or $t\text{-BuLi}$; BBr_3 ; Brønsted bases; ii) BBr_3 or Bi_3 ; with or without Brønsted bases; (b) intermediate-mediated post-modification: iii) B_2Pin , $[\text{Ir}(\text{COD})(\text{OCH}_3)]_2$, dtbpy, THF, reflux; iv) NBS , CHCl_3 ; and c) one-step post-modification: v) S_8 , I_2 , o-DCB; and vi) PhP(O)(H)(OH) , Tf_2O , DMAP, DCE.

frameworks, thereby effectively overcoming some inherent limitations of de novo synthesis routes. In 2022, our group developed the C–H activation strategy to synthesize the key intermediate DtCzB-Bpin, which enables modular tuning at the LUMO site via Suzuki coupling.^[36] Afterwards, our group introduced the *N*-bromosuccinimide (NBS) bromination strategy to access key intermediates m-Br-BNCz and m-DBr-BNCz, allowing HOMO-site functionalization via Suzuki coupling, accompanied by sterically induced rearrangement.^[37] Unfortunately, in these post-modification strategies, the MR core and functional fragments are connected by freely rotatable single bonds, which increase excited-state structural relaxation, inevitably resulting in spectral broadening.^[38–42] Recently, our group established a one-step sulfur-locking strategy at the HOMO site that induces a pronounced red-shift in emission, offering a facile approach for constructing red-emissive MR-TADF materials.^[43] Nonetheless, the incorporation of the sp²-hybridized sulfur atom forms a linear N– π –S configuration,

which enhances the intramolecular charge-transfer (ICT) state and results in undesirable spectral broadening.^[44–49] Additionally, the increased molecular planarity strengthens $\pi\cdots\pi$ stacking interactions in the solid state, resulting in severe aggregation-caused quenching (ACQ).^[50–53] Therefore, constructing MR-TADF molecules that simultaneously exhibit high efficiency, narrowband emission, and suppressed ACQ through a simple and efficient one-step post-functionalization strategy remains a significant challenge.

Herein, we propose a promising molecular design strategy involving a one-step phosphine oxide (P=O) post-modification to embed the P=O unit into MR-TADF skeletons (Scheme 1). First, this synthetic route is metal-free, high-yielding, and provides a viable and universal approach for expanding the structural diversity of MR-TADF systems.^[54–57] Second, the insertion of P=O lock enhances the rigidity of the π -conjugation plane and alleviates hydrogen–hydrogen repulsion, resulting in narrowband emission and reduced nonradiative transition process.^[58,59] Third, the

oxygen atom of the P=O moiety is positioned outside the MR π -conjugated plane, exhibiting $n \rightarrow \pi^*$ transition character in the excited state, which enhances spin-orbit coupling (SOC) and facilitates spin-flip process.^[60–64] Finally, the trigonal pyramidal geometry arising from the sp³-hybridized P atom introduces steric hindrance, which mitigates intermolecular interactions and consequently suppresses ACQ and spectral broadening.^[65–72] Based on these considerations, we developed the first B/N/P=O fused MR-TADF emitters, PO-BCzBN and PO-tFBN, which exhibit photoluminescence emission peaks (λ_{PLS}) at 466 and 493 nm with narrow FWHMs of 21 nm (0.12 eV) and 23 nm (0.12 eV) in solution, high photoluminescence quantum yields (Φ_{PLS}) of 98% and 99%, rapid reverse intersystem crossing rates (k_{RISC}) of 2.0×10^4 and 2.1×10^4 s⁻¹ and effectively suppressed concentration quenching and spectral broadening in film state. The sensitizer-free OLEDs with PO-BCzBN and PO-tFBN as emitters achieve maximum external quantum efficiencies (EQE_{max}) of 34.2% (electroluminescence emission peaks, $\lambda_{EL} = 476$ nm, FWHM = 25 nm) and 35.8% ($\lambda_{EL} = 496$ nm, FWHM = 26 nm), respectively.

Results and Discussion

Starting from readily accessible and reported BCz-BN and tFBN, PO-BCzBN and PO-tFBN are synthesized through a simple and effective one-step metal-free reaction.^[73–75] By employing an inexpensive phosphinic acid (PhP(O)(H)(OH)) as the electrophilic reagent and trifluoromethanesulfonic anhydride (Tf₂O) as the catalyst, the double C–P bonds are formed through inter- and intramolecular phospha-Friedel–Crafts (PFC) reactions at the HOMO-active positions. The molecular structures of the target compounds are comprehensively characterized using ¹H, ³¹P, and ¹³C nuclear magnetic resonance (NMR) spectroscopy (Figures S1–S6, Supporting Information), mass spectrometry (Figures S7 and S8) and single-crystal X-ray diffraction analysis (Table S1). Thermogravimetric analysis (TGA) reveals high decomposition temperatures (T_d , defined as 5% weight loss) of 449.2 °C for PO-BCzBN and 463.8 °C for PO-tFBN (Figure S9), indicating excellent thermal stability suitable for vacuum-deposited OLED fabrication. Based on the cyclic voltammetry (CV) results (Figure S10), the LUMO energy levels of BCz-BN, PO-BCzBN and PO-tFBN are –2.74, –2.77, and –2.76 eV, respectively, while their HOMO energy levels are –5.36, –5.49, and –5.40 eV, respectively. Compared to BCz-BN, the formation of linear P=O– π –N structure in PO-BCzBN reduces the electron-donating ability of the N atom, leading to a more pronounced decrease in the HOMO energy level, relative to the decrease in the LUMO level. Consequently, a blue-shifted emission can be anticipated. Further, the incorporation of the electron-donating *tert*-butylfluorene (tF) unit significantly raises the HOMO level, while having minimal effect on the LUMO. These observations are consistent with the theoretical calculations presented below.

To elucidate the S₀ electronic structures of BCz-BN, PO-BCzBN, and PO-tFBN, density functional theory (DFT) calculations are performed using the Gaussian 16 package

at the B3LYP/6–31G(d,p) level.^[76–81] As shown in Figure 1a, the LUMOs of all three compounds are primarily localized on the BCz-BN core, with similar energy levels of –1.73, –1.89, and –1.87 eV, respectively. Compared to BCz-BN, the HOMO of PO-BCzBN remains largely localized on the BCz-BN core but shows partial extension into the P=O unit, resulting in a lower HOMO energy (–5.28 eV) and a larger energy gap ($E_{gap} = 3.39$ eV) relative to BCz-BN (HOMO = –5.07 eV, $E_{gap} = 3.34$ eV). Further, the introduction of the electron-donating tF unit raises the HOMO level in PO-tFBN while maintaining a comparable LUMO, thereby reducing the E_{gap} to 3.24 eV. These results indicate that electron-withdrawing substituents at the HOMO site induce a hypsochromic shift in emission, whereas electron-donating groups cause a bathochromic shift. The oscillator strengths ($f_{S_0 \rightarrow S_1}$) for the S₀→S₁ transition are calculated to be 0.4042, 0.3837, and 0.3119 for BCz-BN, PO-BCzBN, and PO-tFBN, respectively, indicating their high radiative transition rate (k_r) associated with the short-range charge-transfer (SRCT) character.

To accurately estimate the excited-state energies, high-level quantum chemical calculations are carried out using the spin-component scaled second-order approximate coupled-cluster (SCS-CC2) method (Figure 1b).^[82,83] The S₁/T₁ energies for BCz-BN, PO-BCzBN, and PO-tFBN are calculated to be 3.03/2.92, 3.07/2.95, and 2.86/2.77 eV, respectively. This results in small ΔE_{ST} values of 0.11, 0.12 and 0.09 eV for BCzBN, PO-tFBN, and PO-BCzBN, which are conducive to the RISC process from T₁ state to S₁ state. To further understand the nature of the excited states, hole-electron distribution analyses are conducted for the S₁ and T₁–T₃ states of the three molecules (Figures 1c and S11).^[84,85] BCz-BN exhibits only $\pi \rightarrow \pi^*$ transitions in the S₁ and T₁–T₃ states with minimal differences in hole-electron distributions, and possesses relatively small SOC matrix elements of 0.04, 0.03 and 0.16 cm^{–1} for $\langle S_1 | \hat{H}_{SOC} | T_1 \rangle$, $\langle S_1 | \hat{H}_{SOC} | T_2 \rangle$ and $\langle S_1 | \hat{H}_{SOC} | T_3 \rangle$, respectively. By contrast, the excited states of PO-BCzBN and PO-tFBN remain predominantly characterized by $\pi \rightarrow \pi^*$ transition, yet exhibit additional contributions from $n \rightarrow \pi^*$ transitions on the oxygen atom. As a result, the $\langle S_1 | \hat{H}_{SOC} | T_1 \rangle$, $\langle S_1 | \hat{H}_{SOC} | T_2 \rangle$ and $\langle S_1 | \hat{H}_{SOC} | T_3 \rangle$ values for PO-BCzBN and PO-tFBN increase to 0.08/0.10/0.47 and 0.06/0.29/0.46 cm^{–1}, respectively. The enhanced SOC is attributed to the combined effects of $n \rightarrow \pi^*$ contributions and the altered hole-electron distributions, both of which facilitate spin-flip process through increased orbital angular momentum interactions.^[60–64] In addition, we also analyzed the structural reorganization energies (λ) between the S₀ and S₁ states to assess the influence of introducing P=O lock on the emission properties (Figure S12). The λ values of BCz-BN, PO-BCzBN, and PO-tFBN are estimated to be 0.0693, 0.0697, and 0.0897 eV, respectively.^[86] This indicates that the introduction of the P=O unit has negligible effect on the FWHM.

The influence of the P=O unit on molecular geometry and packing mode is clearly revealed by single-crystal structures.^[87] For comparison, the single-crystal structure of BCz-BN is selected.^[88] All crystallographic data are summarized in Table S1. The embedded sp³-hybridized P atom in PO-BCzBN and PO-tFBN adopt typical trigonal

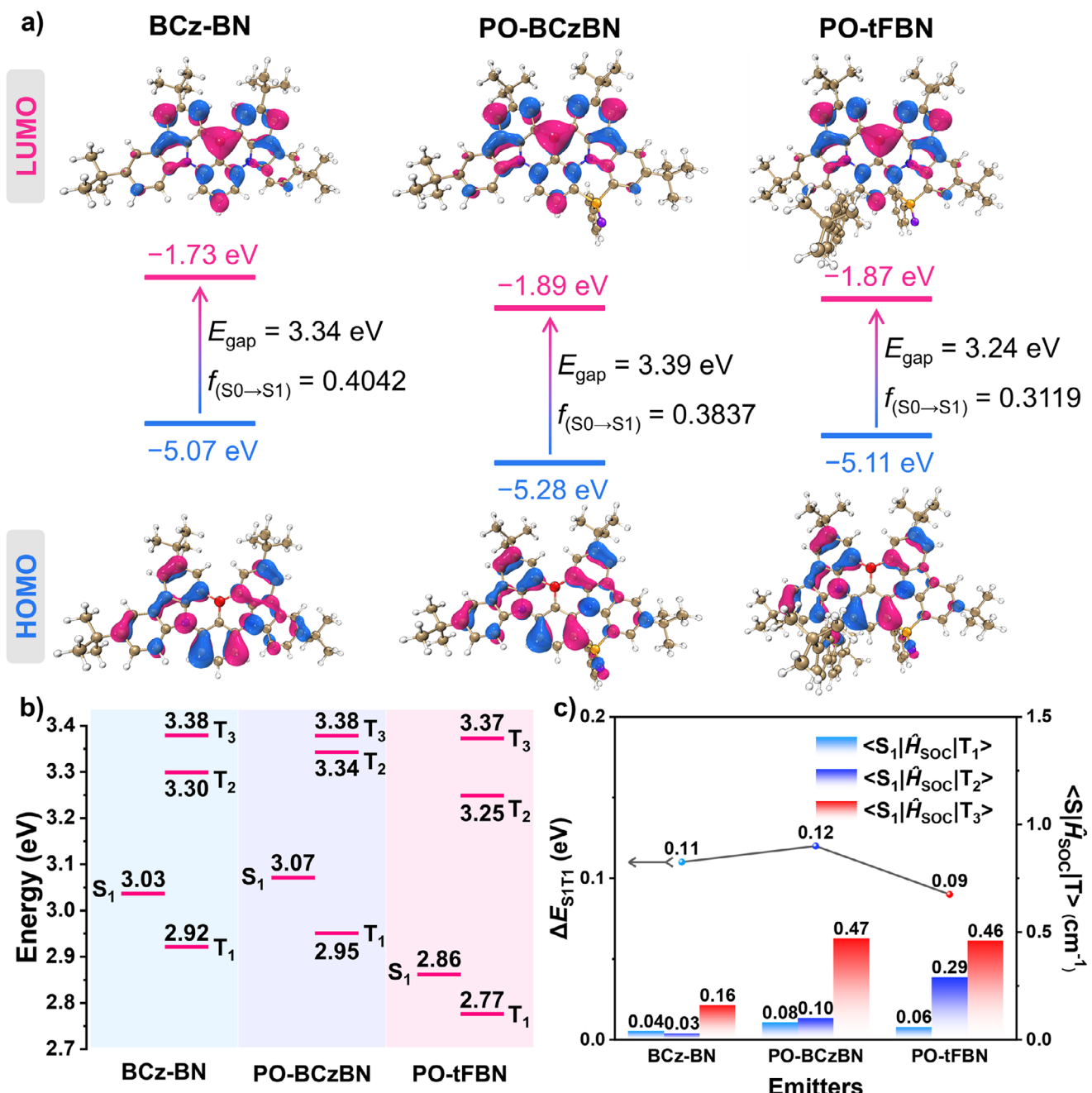


Figure 1. a) Calculated HOMO and LUMO distributions, HOMO–LUMO energy level gaps and the f values of BCz-BN, PO-BCzBN and PO-tFBN; b) Excited-state energies alignment of BCz-BN, PO-BCzBN and PO-tFBN at the SCS-CC2 method; and c) SOC constants of BCz-BN, PO-BCzBN and PO-tFBN at B3LYP/6-31G(d,p) level.

pyramidal geometries and slightly deviate from the central six-membered azaphosphinine plane, with out-of-plane displacements of 0.11 and 0.28 Å, respectively, suggesting their slightly crooked molecular structures relative to BCz-BN core. The C–P bond lengths range from 1.78–1.81 Å, while the P=O bond measures 1.48 Å, consistent with typical phosphine oxide structures (Figure S13). As presented in Figure 2, the dihedral angles of the B/B', A/C and A/C' rings in BCz-BN are 12.16°, 8.61°, and 18.30°, respectively. In comparison, the corresponding angles in PO-BCzBN and PO-

tFBN are 5.73°/6.71°/16.40° and 2.82°/3.61°/4.75°, respectively. This verifies that due to the insertion of P=O lock, the MR-core become more rigid and planar, which can be attributed to the alleviation of the steric repulsion between proximate hydrogen atoms. In the crystal packing, BCz-BN assemble into columnar parallel π -stacked structures with distance of 3.668 Å. Due to the presence of C–H···O hydrogen bonding (distance: 2.635 Å, angle: 161.32°), PO-BCzBN assembles into antiparallel slipped π -stacked structures with distances of 3.656 Å between R/S-isomers and 3.823 Å between

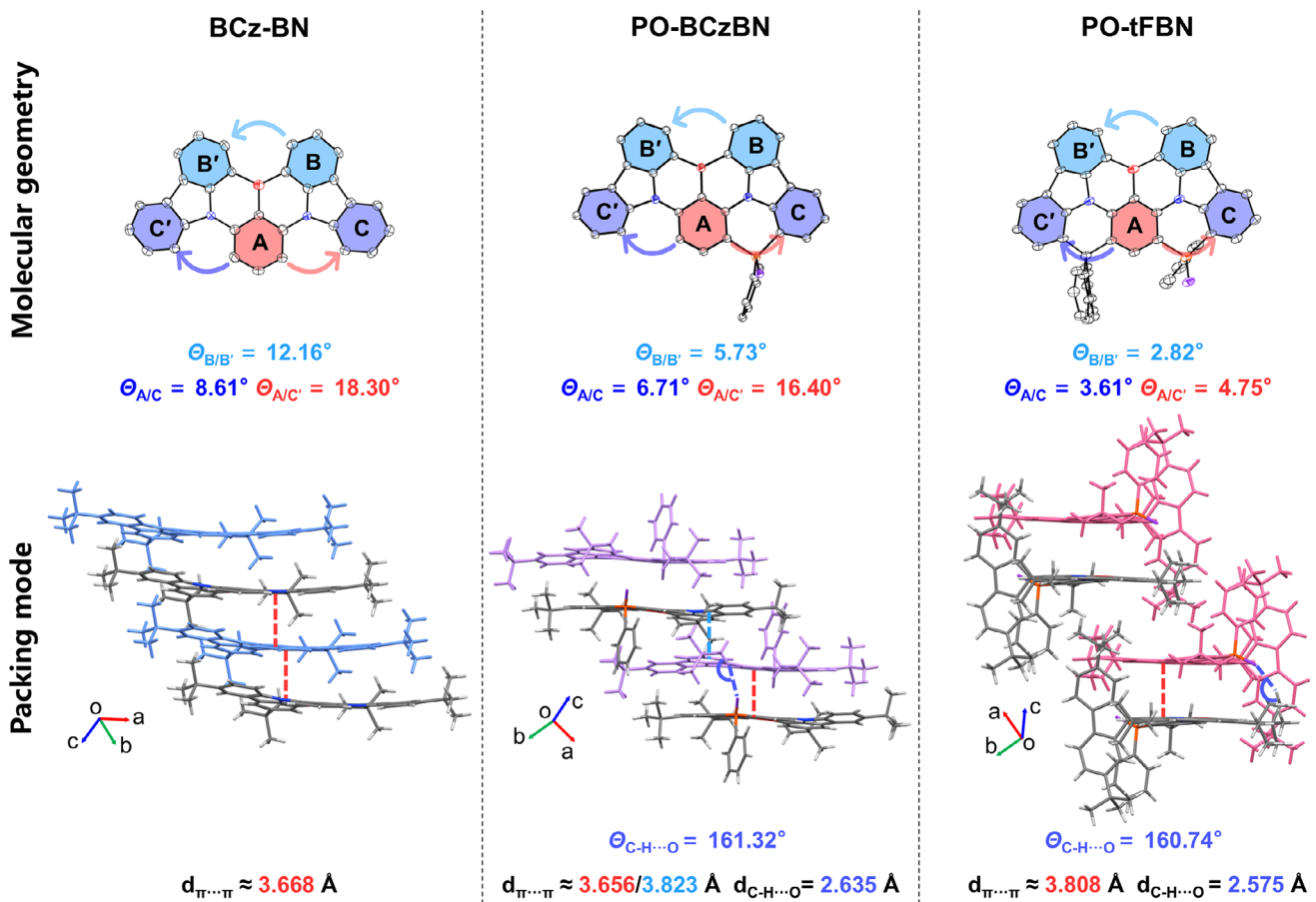


Figure 2. Molecular geometries (with *t*-Bu groups omitted for clarity) and packing modes for the single crystals of BCz-BN, PO-BCzBN, and PO-tFBN.

Table 1: Summary of the photophysical data of BCz-BN, PO-BCzBN, and PO-tFBN.

Emitter	$\lambda_{\text{abs}}^{\text{a})}$ [nm]	$\lambda_{\text{PL}}^{\text{a})}$ [nm]	FWHM ^{a)} [nm/eV]	$\Delta E_{\text{ST}}^{\text{b)}$ [eV]	$\Phi_{\text{PL}}^{\text{c)}$ [%]	$\tau_p^{\text{c)}$ [ns]	$\tau_d^{\text{c)}$ [μs]	$k_r^{\text{c)}$ (10^7 s $^{-1}$)	$k_{\text{nr}}^{\text{c)}$ (10^6 s $^{-1}$)	$k_{\text{ISC}}^{\text{c)}$ (10^7 s $^{-1}$)	$k_{\text{RISC}}^{\text{c)}$ (10^4 s $^{-1}$)
BCz-BN	468	482	22/0.12	0.16	93	6.9	109.9	11.5	12.8	1.8	1.0
PO-BCzBN	454	466	21/0.12	0.18	98	5.3	68.0	13.7	2.8	5.0	2.0
PO-tFBN	478	493	23/0.12	0.15	99	5.7	55.4	14.5	1.5	2.7	2.1

^{a)} Measured in diluted toluene solution at 298 K. ^{b)} Measured in diluted toluene solution at 77 K. ^{c)} Measured in 3 wt% doped films in PhCzBCz.

adjacent dimers. In addition, the locally distorted configuration at the sp^3 -hybridized P-center facilitates significant slip-stacked arrangements between neighboring dimers, thereby preventing long-range interchromophore interactions.^[89–91] In PO-tFBN, C–H···O hydrogen bonding occurs between R/S-isomers, with a bond length of 2.575 Å and a bond angle of 160.74°, inducing an antiparallel slipped π -stacked dimeric arrangement. The incorporation of the tF unit increases the stacking distance to 3.808 Å between R/S-isomers. Meantime, the nearly negligible π ··· π overlap area between adjacent dimers indicates minimal π ··· π interactions, thereby further efficiently suppressing long-range interchromophore coupling.

The UV-vis absorption and PL spectra of BCz-BN, PO-BCzBN, and PO-tFBN are recorded in dilute toluene solutions (1×10^{-5} M) and the corresponding photophysical

data are listed in Table 1. As shown in Figures 3a, S14, and Table S2, BCz-BN, PO-BCzBN and PO-tFBN display intense SRCT absorption bands with maxima at 468, 454 and 478 nm, respectively, accompanied by high molar extinction coefficients (ε) of 5.5×10^4 , 4.7×10^4 , and 2.7×10^4 M $^{-1}$ cm $^{-1}$. In the PL spectrum obtained at room temperature, PO-BCzBN and PO-tFBN exhibit narrowband blue and blue-green emissions with peaks at 466 and 493 nm, and FWHMs of 21 nm (0.12 eV) and 23 nm (0.12 eV), respectively. Such small FWHM values are comparable to that of BCz-BN (22 nm, 0.12 eV). This indicates that the introduction of the sp^3 -hybridized P atom and tF unit does not lead to broadening of FWHM, owing to the enhanced rigidity of the π -conjugation plane. According to the onsets of fluorescence and phosphorescence spectra recorded in toluene at 77 K (Figure S15), the S_1 and T_1 energy levels of PO-BCzBN

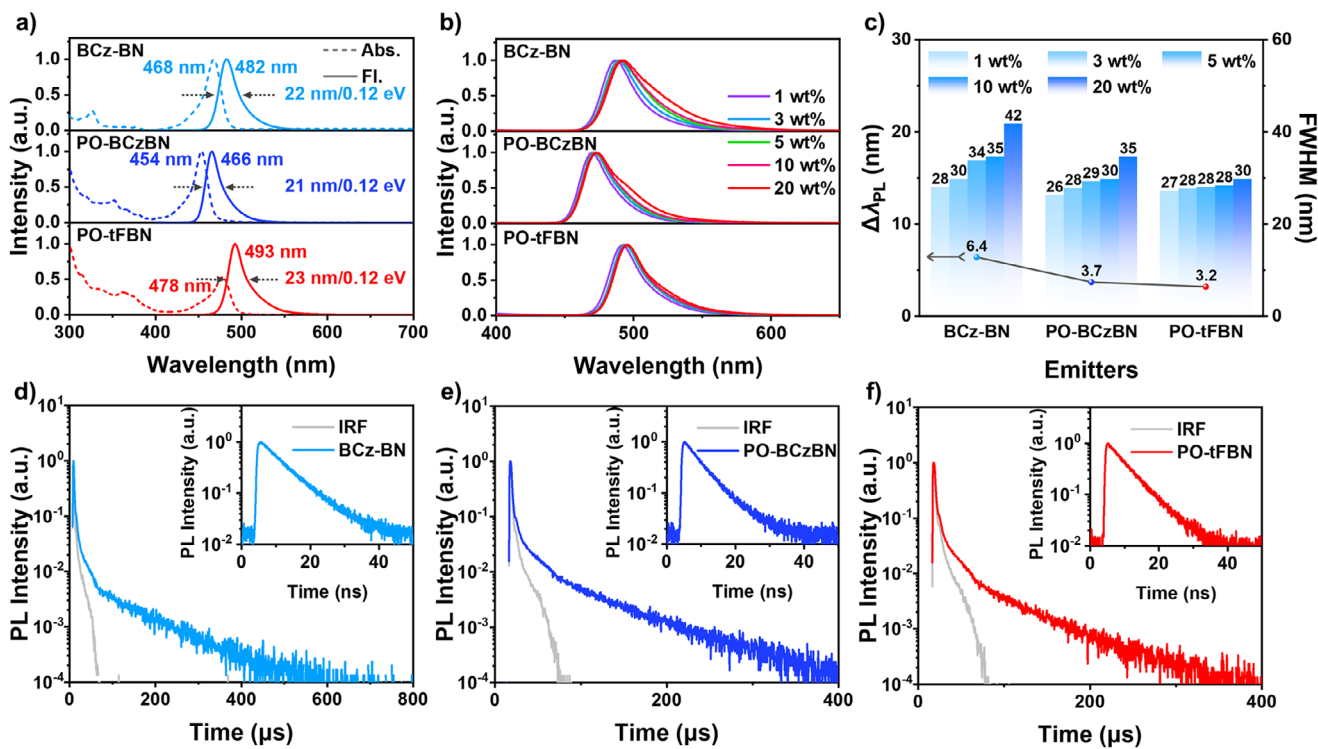


Figure 3. a) UV–vis absorption (Abs.), fluorescence (Fl., measured at 298 K) spectra of BCz-BN, PO-BCzBN and PO-tFBN in toluene (1×10^{-5} M); b) PL spectra of BCz-BN, PO-BCzBN and PO-tFBN in doped films with doping concentrations of 1–20 wt%; c) PL emission peak shift and FWHM of BCz-BN, PO-BCzBN and PO-tFBN in doped films with doping concentrations of 1–20 wt%; transient PL decay curves of d) BCzBN, e) PO-BCzBN, and f) PO-tFBN in PhCzBCz under inert atmosphere.

and PO-tFBN are estimated to be 2.78/2.60 and 2.63/2.48 eV, respectively. Therefore, the ΔE_{ST} values of PO-BCzBN and PO-tFBN are 0.18 and 0.15 eV, respectively, which are comparable to that of BCz-BN (0.16 eV). Additionally, as the solvent polarity increases from nonpolar *n*-hexane to highly polar dichloromethane, slight solvatochromic shifts are observed, consistent with the behavior reported for B/N-based MR-TADF emitters (Figure S16 and Table S3).^[92–94]

To explore the photophysical properties in the solid state, the vacuum-deposited doped thin films are fabricated using a high-energy-gap host, 9-(2-(9-phenyl-9*H*-carbazol-3-yl)phenyl)-9*H*-3,9'-bicarbazole (PhCzBCz), with doping concentrations range from 1 to 20 wt%. As demonstrated in Figures 3b,c and Table S4, the 3 wt%-doped films of BCz-BN, PO-BCzBN and PO-tFBN exhibit narrowband blue and blue-green emissions with peak wavelengths of 488.9, 470.5 and 494.4 nm, FWHMs of 29.8, 27.8, and 27.7 nm and high Φ_{PLS} of 93%, 98%, and 99%, respectively. The slight emission bathochromic shifts and broadening in FWHMs compared to the solution state are attributed to solid-state solvatochromic effects and increased doping levels. As the doping concentration increases from 1 to 20 wt%, the emission spectra of BCz-BN-doped films exhibit clear red shifts (λ_{PLS} from 486.6 to 493.0 nm) and broadenings (FWHMs from 28.0 to 41.8 nm), which primarily originates from excimer formation, as previously demonstrated (Figure 3c and Table S4).^[95] Fortunately, the incorporation of the sp³-hybridized P atom effectively suppresses long-range interchromophore interac-

tions. As a result, the emission spectra of PO-BCzBN in 1–20wt% doped films exhibit only slight red shifts from 469.6 to 473.3 nm, accompanied by modest FWHMs increase from 26.3 to 34.6 nm, indicating enhanced resistance to concentration-dependent spectral broadening. Additionally, the introduction of tF unit in PO-tFBN further increases the $\pi \cdots \pi$ stacking distance, thereby effectively suppressing ACQ. As a consequence, PO-tFBN displays the minimum red shifts from 492.6 to 495.8 nm and increase in FWHMs from 27.2 to 29.8 nm. In highly doped films, the Φ_{PLS} of all three molecules exhibit a decreasing trend. Nevertheless, even at a doping concentration of 20 wt%, PO-BCzBN and PO-tFBN maintain relatively high Φ_{PLS} of 85% and 87%, respectively, compared with 80% for BCz-BN, further demonstrating the suppression of ACQ (Table S4).^[96] To assess the TADF property, the transient PL measurements are performed at room temperature (Figures 3d–f, S17, and 18). As expected, PO-BCzBN and PO-tFBN exhibit distinct bi-component decay profiles, comprising a prompt fluorescence (τ_p) component and a delayed fluorescence (τ_d) component, similar to BCz-BN. The τ_p and τ_d lifetimes of PO-BCzBN and PO-tFBN in 3 wt% doped films are measured to be 5.3 ns/68.0 μ s and 5.7 ns/55.4 μ s, respectively. In contrast, BCz-BN displays a longer τ_d lifetime of 109.9 μ s. The shorter τ_d lifetimes observed in PO-BCzBN and PO-tFBN are attributed to their enhanced SOC matrix elements at comparable ΔE_{ST} levels, which are highly favorable for promoting the RISC process.^[97] Furthermore, temperature-dependent

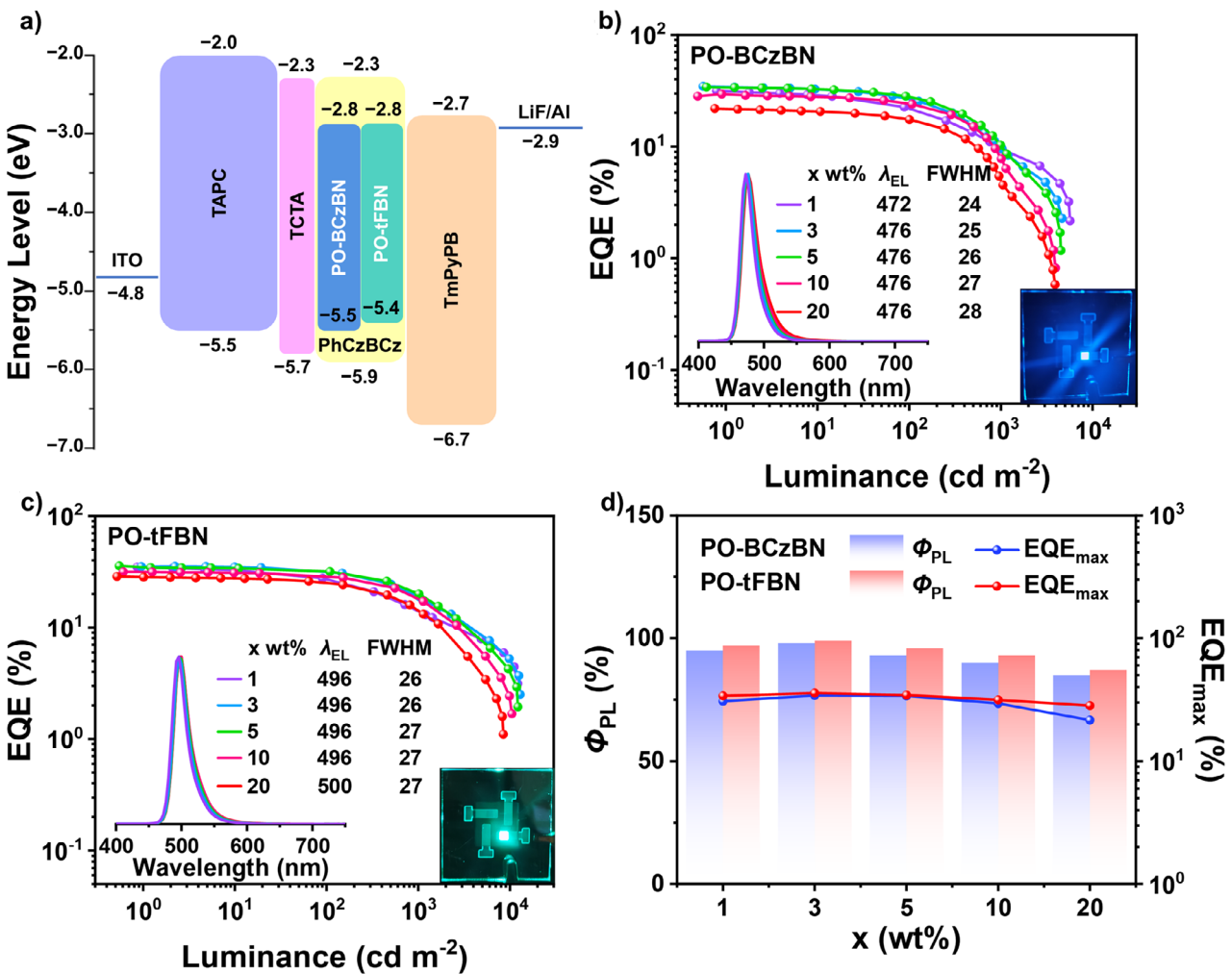


Figure 4. EL characteristics of devices based on PO-BCzBN and PO-tFBN: a) corresponding device structures and energy level diagrams; EQE-luminance curves of b) PO-BCzBN, and c) PO-tFBN (inset: EL spectra with doping concentrations range from 1 to 20 wt% and images taken with 3 wt%-based devices); d) Φ_{PL} s and EQE_{max} s of PO-BCzBN and PO-tFBN in doped films with different doping concentrations of 1–20 wt%.

transient PL decay spectra are recorded (Figure S19). As the temperature increases from 100 to 300 K, the proportion of the τ_d component gradually increases, further confirming the typical TADF characteristics of PO-BCzBN and PO-tFBN.^[98,99] Kinetic parameters are extracted based on the Φ_{PL} , τ_p , and τ_d components, following previously reported methods.^[100–103] The k_{RISC} s of PO-BCzBN and PO-tFBN are estimated to be 2.0×10^4 and $2.1 \times 10^4 \text{ s}^{-1}$, respectively—approximately twice that of BCz-BN ($1.0 \times 10^4 \text{ s}^{-1}$). In addition, while maintaining a relatively high k_{rs} ($> 10^8 \text{ s}^{-1}$), the non-radiative decay rate constants (k_{nr}) of PO-BCzBN and PO-tFBN decreased to 2.8×10^6 and $1.5 \times 10^6 \text{ s}^{-1}$, respectively. In contrast, the k_{nr} of BCz-BN is $1.3 \times 10^7 \text{ s}^{-1}$.^[104] These photophysical data, summarized in Tables 1 and S4, strongly support the effectiveness of our proposed strategy for developing MR-TADF emitters that simultaneously exhibit high Φ_{PL} s, narrowband emission, and suppressed concentration quenching.

The excellent photophysical properties of PO-BCzBN and PO-tFBN prompt us to explore their potential in electroluminescent device applications.

Vacuum-deposited OLEDs are assembled using binary emitting layers (EMLs) comprising PO-BCzBN or PO-tFBN as the emitters and PhCzBCz as the host. The optimized device architecture is as follows: indium tin oxide (ITO)/1,1-bis[(di-4-tolylamino)phenyl]cyclohexane (TAPC, 50 nm)/tris(4-carbazolyl-9-ylphenyl)amine (TCTA, 5 nm)/PhCzBCz: x wt% emitters (30 nm)/(3,3'-[5'-[3-(3-pyridinyl)phenyl][1,1':3',1''-terphenyl]-3,3''-diyl]bispyridine) (TmPyPB, 30 nm)/lithium fluoride (LiF, 1 nm)/aluminum (Al, 100 nm) ($x = 1, 3, 5, 10, 20$). Here, ITO and Al served as the anode and cathode, respectively. TAPC, TCTA and TmPyPB function as the hole-transporting layer (HTL), electron-blocking layer (EBL) and electron-transporting layer (ETL), respectively. LiF acts as the electron-injection layer (EIL). The corresponding device structures, energy level diagrams, and molecular structures of the materials used are illustrated in Figures 4a,b. All relevant device data are summarized in Figures 4, S20–22, and Table 2.

All devices provide similarly low turn-on voltages (recorded at 1 cd m^{-2}) ranging from 2.6 to 3.0 V, attributed to well-matched energy levels across the functional layers

Table 2: Summary of the EL data of the devices based on PO-BCzBN and PO-tFBN.

Emitters	x [wt%]	λ_{EL} ^{a)} [nm]	FWHM ^{b)} [nm]	V_{on} ^{c)} [V]	L_{max} ^{d)} [cd m ⁻²]	CE_{max} ^{e)} [cd A ⁻¹]	PE_{max} ^{f)} [lm W ⁻¹]	$EQE_{max/100/1000}$ ^{g)} [%]	Roll-off _{100/1000} ^{h)} [%]	CIE ⁱ⁾ (x, y)
PO-BCzBN	1	472	24	2.9	5668	30.0	31.9	30.7/21.9/9.5	28.7/69.1	(0.11, 0.14)
	3	476	25	2.8	4626	37.0	40.7	34.2/26.5/9.8	22.5/71.3	(0.11, 0.16)
	5	476	26	2.8	4503	37.9	42.4	33.9/27.8/10.1	18.0/70.2	(0.11, 0.17)
	10	476	27	2.7	3934	36.1	42.0	29.5/24.1/8.1	18.3/72.5	(0.11, 0.19)
	20	476	28	2.7	3897	28.8	33.6	21.6/17.4/5.0	19.4/76.9	(0.11, 0.22)
PO-tFBN	1	496	26	3.0	12 170	73.5	78.3	34.0/27.2/14.0	20.0/58.8	(0.09, 0.50)
	3	496	26	2.8	11 710	81.7	90.9	35.8/31.7/19.6	11.5/45.3	(0.09, 0.55)
	5	496	27	2.7	12 190	81.1	91.9	34.5/31.9/20.2	7.5/41.4	(0.10, 0.56)
	10	496	27	2.7	10 460	75.8	87.7	31.5/28.5/18.1	9.5/42.5	(0.10, 0.57)
	20	500	27	2.6	8441	68.4	80.3	28.3/24.8/14.0	12.4/50.5	(0.11, 0.57)

^{a)} EL emission peak. ^{b)} Full-width at half-maximum. ^{c)} Turn-on voltage at 1 cd m⁻². ^{d)} Maximum luminance. ^{e)} Maximum current efficiency. ^{f)} Maximum power efficiency. ^{g)} Maximum external quantum efficiency, and values at 100 and 1000 cd m⁻², respectively. ^{h)} Efficiency roll-off values at 100 and 1000 cd m⁻², respectively. ⁱ⁾ Commission Internationale de l'Eclairage coordinates (value taken at 100 cd m⁻²).

(Table 2). With increasing doping concentrations from 1 to 20 wt%, the PO-BCzBN-based devices show only slight changes in EL spectra, with emission peaks shifting from 472 to 476 nm and FWHMs ranging from 24 to 28 nm, indicating effective suppression of intermolecular interactions. In particular, PO-tFBN-based devices exhibit more outstanding ability to relieve ACQ with emission peaks shifting from 496 to 500 nm and FWHMs of 26 to 27 nm, across the 1–20 wt% doping range. For devices with PO-BCzBN or PO-tFBN as the emitters, EQE_{max}s remain at high levels over a wide range of dopant concentrations. Impressively, PO-tFBN-based devices exhibit higher EQE_{max}s of 28.3%–35.8% across a dopant concentration range of 1–20 wt%, surpassing those of the PO-BCzBN-based counterparts (21.6%–34.2%), which is consistent with the trend observed in Φ_{PLS} (Figure 4d). The optimal EL performance is achieved in devices doped at 3 wt%, exhibiting EQE_{max}s, current efficiencies (CE_{max}s) and power efficiencies (PE_{max}s) of 34.2% and 35.8%, 37.0 and 81.7 cd A⁻¹, and 40.7 and 90.9 lm W⁻¹ for PO-BCzBN- and PO-tFBN-based devices, respectively. Moreover, compared to PO-BCzBN, the PO-tFBN-based device exhibits lower efficiency roll-off with the EQE values of 31.7% and 19.6% at the brightness levels of 100 and 1000 cd m⁻¹, respectively. The suppression of efficiency roll-off is associated with suppressed ACQ, fast k_{RISC} and low k_{nr} of PO-tFBN, which mitigate triplet-related annihilation processes. Compared with existing MR-TADF molecules, our molecular design strategy not only inhibits the ACQ effect and spectral broadening but also reduces efficiency roll-off.^[73–75]

To further improve device performance, the sensitized devices are fabricated using 2,3,5,6-tetrakis(3,6-di-*tert*-butyl-9H-carbazol-9-yl)benzonitrile (4TCzBN) as the sensitizer (Figure S23). 4TCzBN is chosen owing to sufficient spectral overlap between the emission of 4TCzBN and the absorption of PO-BCzBN or PO-tFBN (Figure S24) and fast k_{RISC} (7.4×10^4 s⁻¹), which can facilitate efficient Förster energy transfer.^[105–107] As demonstrated in Figures S25, S26, and Table S5, the sensitized devices doped at 3 wt% exhibited narrowband blue and blue-green emissions at 472 nm (PO-BCzBN) and 496 nm (PO-tFBN), both with FWHM values of 26 nm. The devices based PO-BCzBN and PO-tFBN deliver

enhanced electroluminescent performance, with EQE_{max} of 31.5% and 32.9%, CE_{max} of 38.3 and 74.8 cd A⁻¹, and PE_{max} of 43.8 and 85.5 lm W⁻¹, respectively. Notably, the efficiency roll-offs are further alleviated, with EQE values of 27.8% and 30.1% at 100 cd m⁻², and 18.5% and 23.5% at 1000 cd m⁻², respectively. Furthermore, the operational lifetimes (LT₅₀, time required for the luminance to decay to 50% of its initial value) of PO-BCzBN- and PO-tFBN-based devices are measured to be 0.2 and 0.9 h, respectively, at an initial luminance (L₀) of 1000 cd m⁻² (Figure S27). Compared to PO-BCzBN, the longer lifetime of the PO-tFBN-based device can be attributed to its lower excited-state energies for reducing the risk of photochemical degradation induced by high-energy excitons and the enhanced ability to suppress ACQ for reducing exciton annihilation.^[108]

Conclusion

In summary, we propose an innovative molecular design strategy via a one-step P=O post-modification strategy to construct the first B/N/P=O fused MR-TADF emitters, PO-BCzBN and PO-tFBN. The synthetic route is high-yielding, operationally simple, and avoids the use of metals, offering a feasible pathway for diversifying MR-TADF architectures. Moreover, this strategy introduces a covalent P=O lock, which not only enhances the rigidity of the π -conjugation plane to maintain narrowband emission but also suppresses ACQ through the steric hindrance of the sp³-hybridized P center. Consequently, PO-BCzBN and PO-tFBN exhibit maximum λ_{PLS} at 466 nm and 493 nm in solution with narrow FWHMs of 21 nm (0.12 eV) and 23 nm (0.12 eV), high Φ_{PLS} of 98% and 99%, rapid k_{RISCs} of 2.0×10^4 and 2.1×10^4 s⁻¹ and effectively suppressed concentration quenching in film state. Importantly, the sensitizer-free OLEDs deliver outstanding performance, achieving EQE_{max}s of 21.6%–34.2% and 28.3%–35.8% for PO-BCzBN and PO-tFBN, respectively, within a wide doping concentration range of 1–20 wt%. This study demonstrates that our molecular design strategy can be used as a versatile platform to expand the MR-TADF molecular library and is of significance for the development

of efficient, narrowband and quenching-resistant MR-TADF materials.

Acknowledgements

This work was supported by the National Natural Science Foundation of China (52173165), the National Key R&D Program of China (2020YFA0714601), Open Fund of the Key Lab of Organic Optoelectronics and Molecular Engineering of Ministry of Education (53223000122), and the Fundamental Research Funds for the Central Universities. The authors also thank the support of Laboratory of Flexible Electronics Technology, Tsinghua University.

Conflict of Interests

The authors declare no conflict of interest.

Data Availability Statement

Research data are not shared.

Keywords: Multiple resonance • Organic light-emitting diodes • Phosphine-oxide • Post-modification • Thermally activated delayed fluorescence

- [1] F. Santoro, A. Lami, R. Improta, J. Bloino, V. Barone, *J. Chem. Phys.* **2008**, *128*, 224311.
- [2] F. B. Dias, K. N. Bourdakos, V. Jankus, K. C. Moss, K. T. Kamtekar, V. Bhalla, J. Santos, M. R. Bryce, A. P. Monkman, *Adv. Mater.* **2013**, *25*, 3707–3714.
- [3] I. S. Park, K. Matsuo, N. Aizawa, T. Yasuda, *Adv. Funct. Mater.* **2018**, *28*, 1802031.
- [4] T. Hatakeyama, K. Shiren, K. Nakajima, S. Nomura, S. Nakatsuka, K. Kinoshita, J. Ni, Y. Ono, T. Ikuta, *Adv. Mater.* **2016**, *28*, 2777–2781.
- [5] H. Hirai, K. Nakajima, S. Nakatsuka, K. Shiren, J. Ni, S. Nomura, T. Ikuta, T. Hatakeyama, *Angew. Chem. Int. Ed.* **2015**, *54*, 13581–13585.
- [6] P. Ma, Y. Chen, Y. Man, Q. Qi, Y. Guo, H. Wang, Z. Li, P. Chang, C. Qu, C. Han, H. Xu, *Angew. Chem. Int. Ed.* **2024**, *63*, e202316479.
- [7] Y. Yuan, X. Tang, X. Y. Du, Y. Hu, Y. J. Yu, Z. Q. Jiang, L. S. Liao, S. T. Lee, *Adv. Optical Mater.* **2019**, *7*, 1801536.
- [8] J. Wei, C. Zhang, D. Zhang, Y. Zhang, Z. Liu, Z. Li, G. Yu, L. Duan, *Angew. Chem. Int. Ed.* **2021**, *60*, 12269–12273.
- [9] C. Qu, Y. Zhu, L. Liang, K. Ye, Y. Zhang, H. Zhang, Z. Zhang, L. Duan, Y. Wang, *Adv. Optical Mater.* **2023**, *11*, 2203030.
- [10] T. Northey, T. J. Penfold, *Org. Electron.* **2018**, *59*, 45–48.
- [11] A. Pershin, D. Hall, V. Lemaur, J. C. Sancho-Garcia, L. Muccioli, E. Zysman-Colman, D. Beljonne, Y. Olivier, *Nat. Commun.* **2019**, *10*, 597.
- [12] S. Madayanad Suresh, D. Hall, D. Beljonne, Y. Olivier, E. Zysman-Colman, *Adv. Funct. Mater.* **2020**, *30*, 1908677.
- [13] J. Kang, S. Kim, S. O. Jeon, H. L. Lee, I. Kim, U. Jo, S. Han, J. Kim, Y. Jung, H. J. Bae, J. S. Kim, H. Choi, J. Y. Lee, *Adv. Optical Mater.* **2025**, *13*, 2403311.
- [14] M. Mamada, M. Hayakawa, J. Ochi, T. Hatakeyama, *Chem. Soc. Rev.* **2024**, *53*, 1624–1692.
- [15] B. Cui, J. Zhou, C. Duan, H. Xu, *Adv. Optical Mater.* **2025**, *13*, 2403295.
- [16] H.-Z. Li, F.-M. Xie, Y.-Q. Li, J.-X. Tang, *J. Mater. Chem. C* **2023**, *11*, 6471–6511.
- [17] R. Braveenth, K. Raagulan, Y.-J. Kim, B.-M. Kim, *Mater. Adv.* **2023**, *4*, 374–388.
- [18] J. Han, Y. Chen, N. Li, Z. Huang, C. Yang, *aggreg.* **2022**, *3*, e182.
- [19] R. K. Konidena, K. R. Naveen, *Adv. Photonics Res.* **2022**, *3*, 2200201.
- [20] H. J. Kim, T. Yasuda, *Adv. Optical Mater.* **2022**, *10*, 2201714.
- [21] K. R. Naveen, H. I. Yang, J. H. Kwon, *Commun. Chem.* **2022**, *5*, 149.
- [22] J. K. Li, X. Y. Chen, Y. L. Guo, X. C. Wang, A. C. Sue, X. Y. Cao, X. Y. Wang, *J. Am. Chem. Soc.* **2021**, *143*, 17958–17963.
- [23] J. Liu, Y. Zhu, T. Tsuboi, C. Deng, W. Lou, D. Wang, T. Liu, Q. Zhang, *Nat. Commun.* **2022**, *13*, 4876.
- [24] Y. Liu, X. Xiao, Z. Huang, D. Yang, D. Ma, J. Liu, B. Lei, Z. Bin, J. You, *Angew. Chem. Int. Ed.* **2022**, *61*, e202210210.
- [25] X.-C. Fan, K. Wang, Y.-Z. Shi, Y.-C. Cheng, Y.-T. Lee, J. Yu, X.-K. Chen, C. Adachi, X.-H. Zhang, *Nat. Photonics* **2023**, *17*, 280–285.
- [26] L. Ge, W. Zhang, Y. H. Hao, M. Li, Y. Liu, M. Zhou, L. S. Cui, *J. Am. Chem. Soc.* **2024**, *146*, 32826–32836.
- [27] F. Zhang, V. Brancaccio, F. Saal, U. Deori, K. Radacki, H. Braunschweig, P. Rajamalli, P. Ravat, *J. Am. Chem. Soc.* **2024**, *146*, 29782–29791.
- [28] L. Li, T. Huang, Y. Xu, Y. Qu, W. Cui, L. Xu, C. Li, Y. Wang, *Angew. Chem. Int. Ed.* **2025**, *64*, e202504002.
- [29] K. Di, R. Guo, Y. Wang, Y. Lv, H. Su, Q. Zhang, B. Yang, L. Wang, *J. Mater. Chem. C* **2023**, *11*, 6429–6437.
- [30] K. Zhang, X. Wang, Y. Chang, Y. Wu, S. Wang, L. Wang, *Angew. Chem. Int. Ed.* **2023**, *62*, e202313084.
- [31] R. W. Weerasinghe, S. Madayanad Suresh, D. Hall, T. Matulaitis, A. M. Z. Slawin, S. Warriner, Y.-T. Lee, C.-Y. Chan, Y. Tsuchiya, E. Zysman-Colman, C. Adachi, *Adv. Mater.* **2024**, *36*, e2402289.
- [32] T. Feng, X. Nie, D. Liu, L. Wu, C. Y. Liu, X. Mu, Z. Xin, B. Liu, H. Qi, J. Zhang, W. Li, S. J. Su, Z. Ge, *Angew. Chem. Int. Ed.* **2025**, *64*, e202415113.
- [33] Z. Yang, D. Liu, X. Cheng, T. Wang, Z. Li, G. X. Yang, Z. Chen, J. Hu, Y. Fu, X. Nie, Y. Ren, Y. Zeng, Y. Chen, K. Liu, M. Li, S. J. Su, *Angew. Chem. Int. Ed.* **2025**, *64*, e202423602.
- [34] X. Wu, S. Ni, C.-H. Wang, W. Zhu, P.-T. Chou, *Chem. Rev.* **2025**, *125*, 6685–6752.
- [35] M. Mamada, M. Horiuchi, J. Hao, N. Matsuno, K. Tanaka, K. R. Naveen, M. Hayakawa, J. Ochi, S. Oda, Y. Kondo, T. Hatakeyama, *Angew. Chem. Int. Ed.* **2025**, *64*, e202509606.
- [36] Y. Xu, C. Li, Z. Li, J. Wang, J. Xue, Q. Wang, X. Cai, Y. Wang, *CCS Chem* **2022**, *4*, 2065–2079.
- [37] Q. Wang, Y. Xu, T. Yang, J. Xue, Y. Wang, *Adv. Mater.* **2023**, *35*, e2205166.
- [38] F. Liu, Z. Cheng, L. Wan, Z. Feng, H. Liu, H. Jin, L. Gao, P. Lu, W. Yang, *Small* **2022**, *18*, e2106462.
- [39] Y. K. Qu, D. Y. Zhou, F. C. Kong, Q. Zheng, X. Tang, Y. H. Zhu, C. C. Huang, Z. Q. Feng, J. Fan, C. Adachi, L. S. Liao, Z. Q. Jiang, *Angew. Chem. Int. Ed.* **2022**, *61*, e202201886.
- [40] W. C. Guo, W. L. Zhao, K. K. Tan, M. Li, C. F. Chen, *Angew. Chem. Int. Ed.* **2024**, *63*, e202401835.
- [41] W. Zhuang, F. F. Hung, C. M. Che, J. Liu, *Angew. Chem. Int. Ed.* **2024**, *63*, e202406497.
- [42] F. Zheng, X. L. Liu, L. Xing, J. M. Jin, S. Ji, Y. Huo, W. C. Chen, *Angew. Chem. Int. Ed.* **2025**, *64*, e202504057.
- [43] Y. Pu, Q. Jin, Y. Zhang, C. Li, L. Duan, Y. Wang, *Nat. Commun.* **2025**, *16*, 332.

- [44] T. Hua, L. Zhan, N. Li, Z. Huang, X. Cao, Z. Xiao, S. Gong, C. Zhou, C. Zhong, C. Yang, *Chem. Eng. J.* **2021**, *426*, 131169.
- [45] Y. X. Hu, J. Miao, T. Hua, Z. Huang, Y. Qi, Y. Zou, Y. Qiu, H. Xia, H. Liu, X. Cao, C. Yang, *Nat. Photonics* **2022**, *16*, 803–810.
- [46] Q. Li, Y. Wu, Q. Yang, S. Wang, S. Shao, L. Wang, *ACS Appl. Mater. Interfaces* **2022**, *14*, 49995–50003.
- [47] I. S. Park, H. Min, T. Yasuda, *Angew. Chem. Int. Ed.* **2022**, *61*, e202205684.
- [48] J. Wang, N. Li, C. Zhong, J. Miao, Z. Huang, M. Yu, Y. X. Hu, S. Luo, Y. Zou, K. Li, C. Yang, *Adv. Mater.* **2023**, *35*, e2208378.
- [49] J. Szumilas, C. H. Ryoo, M. Mońska, P. Bojarski, S. Y. Park, I. E. Serdiuk, *J. Mater. Chem. C* **2025**, *13*, 8043–8053.
- [50] Y. Kondo, K. Yoshiura, S. Kitera, H. Nishi, S. Oda, H. Gotoh, Y. Sasada, M. Yanai, T. Hatakeyama, *Nat. Photonics* **2019**, *13*, 678–682.
- [51] P. Jiang, J. Miao, X. Cao, H. Xia, K. Pan, T. Hua, X. Lv, Z. Huang, Y. Zou, C. Yang, *Adv. Mater.* **2022**, *34*, e2106954.
- [52] D. Chen, H. Wang, D. Sun, S. Wu, K. Wang, X.-H. Zhang, E. Zysman-Colman, *Adv. Mater.* **2024**, *36*, e2412761.
- [53] R. J. Wang, Y. L. Wu, Y. K. Li, W. C. Chen, Z. X. Lian, P. Y. Zheng, K. J. Shen, L. Zhou, Z. Wang, X. L. Liu, H. Bi, Y. Wang, Y. Huo, *ACS Appl. Mater. Interfaces* **2025**, *17*, 32732–32741.
- [54] Y. Unoh, K. Hirano, M. Miura, *J. Am. Chem. Soc.* **2017**, *139*, 6106–6109.
- [55] K. Nishimura, K. Hirano, M. Miura, *Org. Lett.* **2019**, *21*, 1467–1470.
- [56] K. Nishimura, K. Hirano, M. Miura, *Org. Lett.* **2020**, *22*, 3185–3189.
- [57] Z. Liu, L. Meng, Y. Jiang, C. Li, H. Gu, K. Zhao, J. Zhang, H. Meng, Y. Ren, *J. Am. Chem. Soc.* **2025**, *147*, 3650–3661.
- [58] X. Wang, L. Wang, G. Meng, X. Zeng, D. Zhang, L. Duan, *Sci. Adv.* **2023**, *9*, eadh1434.
- [59] G. Meng, J. Zhou, T. Huang, H. Dai, X. Li, X. Jia, L. Wang, D. Zhang, L. Duan, *Angew. Chem. Int. Ed.* **2023**, *62*, e202309923.
- [60] Z. Yang, G. X. Yang, S. Jiang, M. Li, W. Qiu, X. Peng, C. Shen, Y. Gan, K. Liu, D. Li, S. J. Su, *Adv. Opt. Mater.* **2024**, *12*, 2301711.
- [61] Y. C. Cheng, X. Tang, K. Wang, X. Xiong, X. C. Fan, S. Luo, R. Walia, Y. Xie, T. Zhang, D. Zhang, J. Yu, X. K. Chen, C. Adachi, X. H. Zhang, *Nat. Commun.* **2024**, *15*, 731.
- [62] L. Chen, P. Zou, J. Chen, L. Xu, B. Z. Tang, Z. Zhao, *Nat. Commun.* **2025**, *16*, 1656.
- [63] Y. C. Cheng, R. Walia, T. Y. Zhang, H. Wang, X. Xiong, J. Yu, X. C. Fan, X. K. Chen, K. Wang, X. H. Zhang, *Adv. Opt. Mater.* **2025**, *13*, 2402891.
- [64] R. Walia, X. Fan, L. Mei, W. Guo, K. Wang, C. Adachi, X. K. Chen, X. H. Zhang, *Angew. Chem. Int. Ed.* **2025**, *64*, e202503371.
- [65] J. Bian, S. Chen, L. Qiu, R. Tian, Y. Man, Y. Wang, S. Chen, J. Zhang, C. Duan, C. Han, H. Xu, *Adv. Mater.* **2022**, *34*, e2110547.
- [66] S. Chen, Y. Wang, J. Lin, R. Tian, S. Li, Y. Man, S. Chen, J. Zhang, C. Duan, C. Han, H. Xu, *Chem. Eng. J.* **2024**, *489*, 151517.
- [67] J. Dong, Y. Xu, S. Wang, J. Miao, N. Li, Z. Huang, C. Yang, *Chem. Commun.* **2024**, *60*, 6789–6792.
- [68] X.-J. Liao, S. Xing, J.-J. Hu, X.-Z. Wang, Y.-X. Zheng, *CCS Chem.* **2025**, *7*, 2419–2431.
- [69] Y. Wang, Z. Y. Lv, Z. X. Chen, S. Xing, Z. Z. Huo, X. F. Hong, L. Yuan, W. Li, Y. X. Zheng, *Mater. Horiz.* **2024**, *11*, 4722–4729.
- [70] Y.-S. Wang, X. Lu, J.-H. Song, X. Li, X.-D. Tao, L. Meng, X.-L. Chen, C.-Z. Lu, *Chem. Eng. J.* **2024**, *482*, 148865.
- [71] L. Xing, J. Wang, W. C. Chen, B. Liu, G. Chen, X. Wang, J. H. Tan, S. S. Chen, J. X. Chen, S. Ji, Z. Zhao, M. C. Tang, Y. Huo, *Nat. Commun.* **2024**, *15*, 6175.
- [72] X. Xiong, J. Q. Li, T. F. Chen, X. C. Fan, Y. C. Cheng, H. Wang, F. Huang, H. Wu, J. Yu, X. K. Chen, K. Wang, X. H. Zhang, *Adv. Funct. Mater.* **2024**, *34*, 2313726.
- [73] Y. Zhang, D. Zhang, J. Wei, Z. Liu, Y. Lu, L. Duan, *Angew. Chem. Int. Ed.* **2019**, *58*, 16912–16917.
- [74] Y. Xu, Z. Cheng, Z. Li, B. Liang, J. Wang, J. Wei, Z. Zhang, Y. Wang, *Adv. Optical Mater.* **2020**, *8*, 1902142.
- [75] Y. Pu, X. Cai, Y. Qu, W. Cui, L. Li, C. Li, Y. Zhang, Y. Wang, *Angew. Chem. Int. Ed.* **2025**, *64*, e202420253.
- [76] J. Autschbach, T. Ziegler, S. J. A. Van Gisbergen, E. J. Baerends, *J. Chem. Phys.* **2002**, *116*, 6930–6940.
- [77] J. Tomasi, B. Mennucci, R. Cammi, *Chem. Rev.* **2005**, *105*, 2999–3094.
- [78] E. Runge, E. K. U. Gross, *Phys. Rev. Lett.* **1984**, *52*, 997–1000.
- [79] M. J. Frisch, G. W. Trucks, H. B. Schlegel, G. E. Scuseria, M. A. Robb, J. R. Cheeseman, G. Scalmani, V. Barone, B. Mennucci, G. A. Petersson, H. Nakatsuji, M. Caricato, X. Li, H. P. Hratchian, A. F. Izmaylov, J. Bloino, G. Zheng, J. L. Sonnenberg, M. Hada, M. Ehara, K. Toyota, R. Fukuda, J. Hasegawa, M. Ishida, T. Nakajima, Y. Honda, O. Kitao, H. Nakai, T. Vreven, J. A. Montgomery Jr., et al., Gaussian 16, Revision C.01, Gaussian, Inc., Wallingford CT **2016**.
- [80] A. D. Becke, *J. Chem. Phys.* **1993**, *98*, 5648–5652.
- [81] S. Grimme, J. Antony, S. Ehrlich, H. Krieg, *J. Chem. Phys.* **2010**, *132*, 154104.
- [82] M. Kállay, P. R. Nagy, D. Mester, Z. Rolik, G. Samu, J. Csontos, J. Csóka, P. B. Szabó, L. Gyevi-Nagy, B. Hégely, I. Ladányszki, L. Szegedy, B. Ladóczki, K. Petrov, M. Farkas, P. D. Mezei, Á. Ganyecz, *J. Chem. Phys.* **2020**, *152*, 074107–074124.
- [83] MRCC, a quantum chemical program suite (<https://www.mrcc.hu/>)
- [84] T. Lu, F. Chen, *J. Comput. Chem.* **2012**, *33*, 580–592.
- [85] Z. Liu, T. Lu, Q. Chen, *Carbon* **2020**, *165*, 461–467.
- [86] J. R. Reimers, *J. Chem. Phys.* **2001**, *115*, 9103–9109.
- [87] Deposition Numbers 2468403 (for PO-BCzBN), 2468404 (for PO-tFBN) contain the supplementary crystallographic data for this paper. These data are provided free of charge by the joint Cambridge Crystallographic Data Centre and Fachinformationszentrum Karlsruhe (<http://www.ccdc.cam.ac.uk/structures>)
- [88] M. Yang, I. S. Park, T. Yasuda, *J. Am. Chem. Soc.* **2020**, *142*, 19468–19472.
- [89] Y. Zhang, J. Wei, D. Zhang, C. Yin, G. Li, Z. Liu, X. Jia, J. Qiao, L. Duan, *Angew. Chem. Int. Ed.* **2022**, *61*, e202113206.
- [90] G. Chen, J. Wang, W. C. Chen, Y. Gong, N. Zhuang, H. Liang, L. Xing, Y. Liu, S. Ji, H. L. Zhang, Z. Zhao, Y. Huo, B. Z. Tang, *Adv. Funct. Mater.* **2023**, *33*, 2211893.
- [91] L. Guo, W. Cui, L. Li, Y. Pu, K. Wang, P. Zheng, Y. Wang, C. Li, *Adv. Mater.* **2025**, *37*, e2500269.
- [92] D. K. A. Phan Huu, S. Saseendran, R. Dhali, L. G. Franca, K. Stavrou, A. Monkman, A. Painelli, *J. Am. Chem. Soc.* **2022**, *144*, 15211–15222.
- [93] Z. Huang, H. Xie, J. Miao, Y. Wei, Y. Zou, T. Hua, X. Cao, C. Yang, *J. Am. Chem. Soc.* **2023**, *145*, 12550–12560.
- [94] M. Urban, P. H. Marek-Urbán, K. Durka, S. Luliński, P. Pander, A. P. Monkman, *Angew. Chem. Int. Ed.* **2023**, *62*, e202217530.
- [95] J. M. Jin, D. Liu, W. C. Chen, C. Shi, G. Chen, X. Wang, L. Xing, W. Ying, S. Ji, Y. Huo, S. J. Su, *Angew. Chem. Int. Ed.* **2024**, *63*, e202401120.
- [96] S.-J. Wu, X.-F. Fu, D.-H. Zhang, Y.-F. Sun, X. Lu, F.-L. Lin, L. Meng, X.-L. Chen, C.-Z. Lu, *Adv. Mater.* **2024**, *36*, 2401724.
- [97] Y. Wada, H. Nakagawa, S. Matsumoto, Y. Wakisaka, H. Kaji, *Nat. Photonics* **2020**, *14*, 643–649.
- [98] H. Uoyama, K. Goushi, K. Shizu, H. Nomura, C. Adachi, *Nature* **2012**, *492*, 234–238.
- [99] H. J. Cheon, S. J. Woo, S. H. Baek, J. H. Lee, Y. H. Kim, *Adv. Mater.* **2022**, *34*, e2207416.

- [100] B. S. Brunschwig, J. Logan, M. D. Newton, N. Sutin, *J. Am. Chem. Soc.* **1980**, *102*, 5798–5809.
- [101] J.-L. Brédas, D. Beljonne, V. Coropceanu, J. Cornil, *Chem. Rev.* **2004**, *104*, 4971–5004.
- [102] J. E. Norton, J.-L. Brédas, *J. Am. Chem. Soc.* **2008**, *130*, 12377–12384.
- [103] S. Di Motta, E. Di Donato, F. Negri, G. Orlandi, D. Fazzi, C. Castiglioni, *J. Am. Chem. Soc.* **2009**, *131*, 6591–6598.
- [104] M. Yang, S. Shikita, H. Min, I.n. Park, H. Shibata, N. Amanokura, T. Yasuda, *Angew. Chem. Int. Ed.* **2021**, *60*, 23142–23147.
- [105] D. Zhang, M. Cai, Z. Bin, Y. Zhang, D. Zhang, L. Duan, *Chem. Sci.* **2016**, *7*, 3355–3363.
- [106] D. Zhang, M. Cai, Y. Zhang, D. Zhang, L. Duan, *Mater. Horiz.* **2016**, *3*, 145–151.
- [107] G. Meng, J. Zhou, Q. Wang, T. Huang, G. Zhang, L. Duan, D. Zhang, *Adv. Funct. Mater.* **2025**, *35*, 2422973.
- [108] Q. Feng, X. Zheng, H. Wang, H. Zhang, Y. Qian, K. Tan, H. Cao, L. Xie, W. Huang, *Mater. Adv.* **2021**, *2*, 4000–4008.

Manuscript received: August 16, 2025

Revised manuscript received: September 15, 2025

Accepted manuscript online: September 22, 2025

Version of record online: ■■■